Bulk electronic structure of superconducting $LaRu_2P_2$ single crystals measured by soft x-ray angle-resolved photoemission spectroscopy

E. Razzoli,[1] M. Kobayashi,[1,2] V. N. Strocov,[1] B. Delley,[3] Z. Bukowski,[4] J. Karpinski,[4] N. C. Plumb,[1] M. Radovic,[1,5] J. Chang,[1,5] T. Schmitt,[1] L. Patthey,[1] J. Mesot,[1,5] and M. Shi[1]

[1]*Swiss Light Source, Paul Scherrer Institute, CH-5232 Villigen PSI, Switzerland*
[2]*Department of Applied Chemistry, School of Engineering, University of Tokyo, 7-3-1 Hongo, Bunkyo-ku, Tokyo 113-8656, Japan*
[3]*Paul Scherrer Institute, CH-5232 Villigen PSI, Switzerland*
[4]*Laboratory for Solid State Physics, ETH Zürich, CH-8093 Zürich, Switzerland*
[5]*Institut de la Matiere Complexe, EPF Lausanne, CH-1015, Lausanne, Switzerland*

(Dated: March 4, 2013)

We present a soft X-ray angle-resolved photoemission spectroscopy (SX-ARPES) study of the stoichiometric pnictide superconductor $LaRu_2P_2$. The observed electronic structure is in good agreement with density functional theory (DFT) calculations. However, it is significantly different from its counterpart in high-temperature superconducting Fe-pnictides. In particular the bandwidth renormalization present in the Fe-pnictides ($\sim$ 2 - 3) is negligible in $LaRu_2P_2$ even though the mass enhancement is similar in both systems. Our results suggest that the superconductivity in $LaRu_2P_2$ has a different origin with respect to the iron pnictides. Finally we demonstrate that the increased probing depth of SX-ARPES, compared to the widely used ultraviolet ARPES, is essential in determining the bulk electronic structure in the experiment.

PACS numbers: 74.25.Jb, 71.18.+y,74.70.Xa, 79.60.-i

Before the discovery of high-temperature Fe-pnictide superconductors in 2008 [1], superconductivity had been observed in a number of stoichiometric pnictides, with $LaRu_2P_2$ having the highest superconducting transition temperature (T_c) of $\sim$ 4 K [2]. For Fe-pnictides at ambient pressure, most of the undoped compounds (e.g. $BaFe_2As_2$) have an antiferromagnetic (AFM) ground state, and the superconductivity emerges by applying external pressure or through chemical substitution(s). For example, partially substituting Ru for Fe or P for As can turn $BaFe_2As_2$ into superconductors [3, 4]. On the other hand, the fully substituted compounds $LaFe_2P_2$ [5] and MRu_2P_2 (M = Ca, Sr, Ba) are nonsuperconducting down to 1.8 K [2]. Low-temperature superconductivity occurs when Fe is replaced by Ru in $LaFe_2P_2$ or the alkaline-earth atom is replaced by La in MRu_2P_2. This prompts two intriguing questions: What are the differences in their electronic structures that cause Fe-pnictide superconductors to have significantly higher T_c's than superconducting stoichiometric pnictides?; and is the superconducting mechanism the same in both systems? Recent quantum oscillation measurements have indeed shown similarities in the mass enhancement in Fe-pnictides and $LaRu_2P_2$ [6]. However, this technique is intrinsically unable to distinguish between correlations due to electron-electron interactions, which usually renormalize the entire bandwidth, and contributions due to electron-bosonic mode coupling, which is limited to a narrow energy range (of the order of the boson energy) around E_F. It would be particularly interesting to compare the Fermi surface (FS) topologies and electron-electron correlation effects in $LaRu_2P_2$ and Fe-pnictides, since these have been thought to play important roles in the emergence of superconductivity in Fe-pnictides [7].

To address this question we probe the electronic structure of stoichiometric superconducting pnictide $LaRu_2P_2$ using soft X-ray angle-resolved photoemission spectroscopy (SX-ARPES). $LaRu_2P_2$ is isostructural with "122" Fe-pnictide superconductors (e.g. doped $BaFe_2As_2$), whose electronic states so far have been mostly studied by various conventional techniques [7]. We show that both the FS topology and the bandwidth renormalization of $LaRu_2P_2$ are very different from their high-temperature superconducting Fe-pnictide counterparts. We also demonstrate that, compared to ARPES using ultraviolet light as the excitation source (UV-ARPES), the increased photoelectron mean free path of SX-ARPES is essential in determining of the bulk electronic structure of pnictides. We highlight that it will be important to apply SX-ARPES to Fe-pnictides to resolve the controversies in the reported electronic structures obtained by different techniques.

The SX-ARPES experiments were performed at the Advanced Resonant Spectroscopies (ADRESS) beamline at the Swiss Light Source (SLS). Data were collected using p-polarized light with an overall energy resolution on the order of 80 meV. The UV-ARPES experiments were carried out at the Surface and Interface Spectroscopy (SIS) beam line at SLS. The overall energy resolution was about 15 meV. The samples were cleaved *in situ* at 10 K and measured in a vacuum always better than 5×10^{-11} mbar. For details on samples and experimental procedures, see supplemental material [8].

Figure 1 shows the band structure in the Brillouin zone

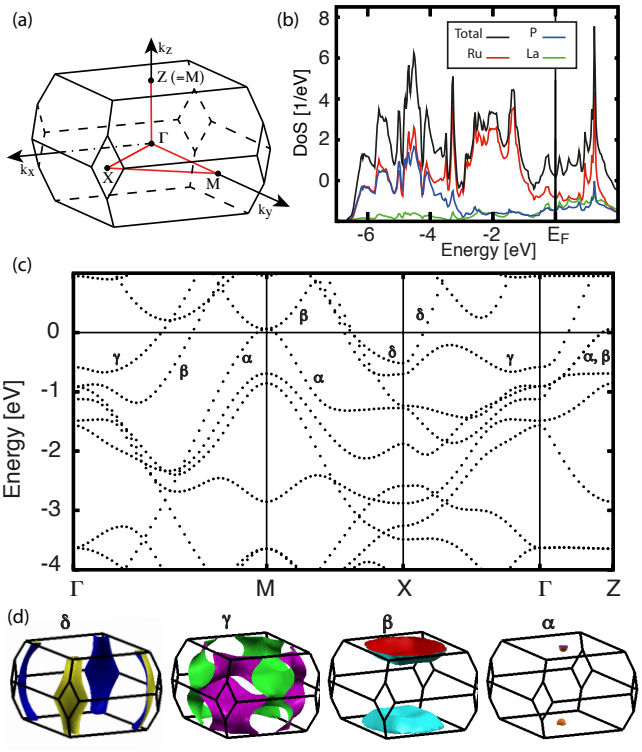

FIG. 1: (Color online) The electronic structure and FS of $LaRu_2P_2$ from DFT calculation. (a) Brillouin zone (BZ) (X = $(\pi/a, \pi/a, 0)$, M = $(0, 2\pi/a, 0)$ and Z = $(0, 0, 2\pi/c)$). (b) Total and partial density of state (DOS) with different atomic characters. (c) The band structure along high symmetry lines. (d) Three-dimensional FS sheets of bands labeled α, β, γ and δ in (c) plotted using XcrysDen visualization package [24].

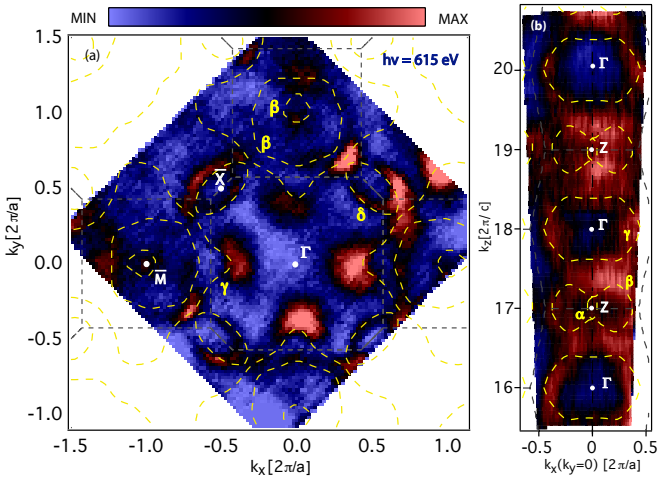

FIG. 2: (Color online) FS intensity maps obtained with SX-ARPES. (a) FS map near the $(k_x,k_y,22\times 2\pi/c)$ plane, taken with $h\nu = 615$ eV. (b) FS map in the $(k_x,0,k_z)$ plane, taken with $h\nu = 300-550$ eV in steps of 5 eV. The maps in (a) and (b) are obtained by integrating ARPES spectral weight in an energy window of $E_F \pm 50$ meV. The superimposed dashed lines are the FS from DFT calculation. $\bar{M}$ ($\bar{X}$) is close to, but slightly different from, M (X) in k_z value.

(BZ) calculated from DFT [9] using the DMol^3 method [10]. Lattice parameters (a = 4.031 Å, c = 10.675 Å) and internal atomic positions (z_{La}=0, z_{Ru}= 0.25, z_P= 0.3593) determined from X-ray diffraction [2] are used in the calculation. DFT total-energy minimization resulted in z_P= 0.36165, which gave only minor changes in the band structure. Near the Fermi level (E_F), α, β and δ have predominant Ru-4d characters (Fig. 1(b)), analogous to the case of $Ba_{1-x}K_xFe_2As_2$ for which the bands within 2 eV of E_F are formed mainly by Fe-3d electrons [11]. The only exception is the γ band, which has admixed Ru-4d and La orbital character. All bands that cross E_F disperse strongly in the k_z direction, hence their FS sheets are highly three-dimensional (Fig. 1(c)-(d)).

In Fig. 2(a)-(b) we plot the ARPES spectral weight mapping at E_F near $(k_x,k_y,22\times 2\pi/c)$ and in the $(k_x,0,k_z)$ planes. The k_z values were extracted by using the free-electron final-state approximation [12] with an inner potential (V_0 = 15 eV) estimated by observing the periodicity of the FS as a function of $h\nu$ and taking into account the photon momentum for our experimental geometry. The superimposed dashed lines are the FS from the DFT calculation. It should be noted that the calculated FS in Fig. 2(a) takes into account the change in k_z as a function of the emission angles of the photoelectrons.

Figure 3(a) shows the ARPES intensity as a function of energy and k along cut 1 in Fig. 4(b). This cut is close to, but slightly deviates from, the Γ-M axis because the k_z values depend on the emitting angles of photoelectrons for a fixed $h\nu$. To trace the detailed dispersion of the α, β and γ bands up to 1.2 eV below E_F, we present in Fig. 3(b), (c) and (d) the second derivative intensity plot along with the bands from the DFT calculation, the momentum distribution curves (MDCs) and the energy distribution curves (EDCs), respectively. The overall agreement between the ARPES spectra and the calculated electronic structure is significant; all features in the ARPES data can be identified from the DFT calculation. A quantitative agreement can be achieved after shifting the γ band up by 100 meV and shifting other bands down slightly for maintaining the charge neutrality of the system. It should be mentioned that, in the study of the electronic structure of $SrFe_2P_2$, shifts of the calculated electronic structure were also required to accurately reproduce the FS from quantum oscillations measurements [13]. The shifts were thought of as a fine tuning of the band structure calculations.

In contrast to Fe-pnictide superconductors, whose bandwidths are renormalized by a factor of 2-3 [14, 15], the dispersions in Fig. 3 can be reproduced by DFT calculation without notable renormalization. To investigate the bandwidth renormalization effect further we have measured the band dispersion along various symmetry lines, as well as many off-symmetry lines in the BZ. Fig-

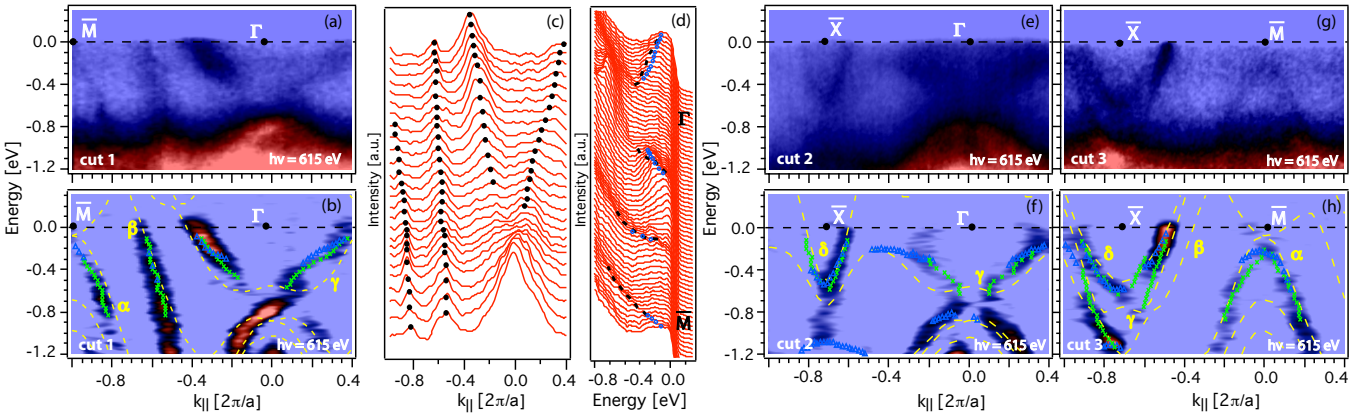

FIG. 3: (Color online) Band dispersion in $LaRu_2P_2$ measured with SX-ARPES. (a), (e) and (g) ARPES spectrum along M-Γ direction (cut 1 Fig. 4 (b)), Γ-X direction (cut 2 Fig. 4 (b)) and the M-X direction (cut 3 Fig. 4 (b)), respectively ($h\nu = 615$ eV). (b),(f) and (h) Second derivatives of the MDCs in (a), (e) and (g), respectively. The DFT band structure (dashed lines), MDC peaks (green crosses) and EDC peaks (blue triangles) are superimposed on the data. (c) MDCs and MDC peaks (black dots) from (a). (d) EDCs and EDC peaks (blue circles) from (a). Dashed lines trace the MDCs dispersion.

ure 3 (e)-(h) shows the ARPES spectra acquired along the Γ-X and M-X directions (cuts 2 and 3 in Figure 4(b)) and their second derivative intensity plots. EDC and MDC peak positions are superimposed on the second derivative intensity plots. As for the α, β and γ bands, the dispersion of the δ band which forms the electron-like FS pocket around the X point can also be well described by the DFT calculation. The good agreement between the electronic structure determined experimentally and that calculated from DFT indicates that the Ru-4d electrons are delocalized in nature, which can be captured well by DFT band calculations.

The negligible bandwidth renormalization indicates that the overall electron-electron correlation is weaker in $LaRu_2P_2$ than in $BaFe_2As_2$. Such a reduction is expected when the ratio of the Coulomb repulsion U to the DFT bandwidth W_{DFT} is decreased [16]. The calculated U is similar in Fe 3d and Ru 4d [17], while our DFT calculations show that the bandwidth of $LaRu_2P_2$ ($\sim$ 10 eV) is substantially larger than that of $BaFe_2As_2$ ($\sim$ 6 eV). This is not surprising since 4d orbitals are much more extended than their 3d counterparts due to higher principal quantum number. We thus conclude that the weaker correlation strength can be attributed to the larger bandwidth of the bare DFT bands of $LaRu_2P_2$. Additionally, the increase in the band filling n due to the replacing Ba with La may further reduce the electron-electron correlations [18]. The observed bandwidth renormalization is consistent with the trend of weakening correlation strength in $Ba(Fe_{1-x}Ru_x)_2As_2$ and $BaFe_2(As_{1-x}P_x)_2$ with increasing x , which are isoelectric substitutions [19, 20]. The general feature of these substitutions, as well as the substitution of Sr with La in $Sr_{1-x}La_xFe_2As_2$ [21], is that at low temperatures upon increasing the concentration of Ru (P, La), superconductivity emerges from an AFM spin-density-wave state, and further substitution drives the system towards a paramagnetic nonsuperconducting metal. The superconductivity occurs only in a finite range of substitution, and the fully substituted compounds ($BaRu_2As_2$, $BaFe_2P_2$) are nonsuperconducting. This suggests that the low-temperature superconductor, $LaRu_2P_2$, belongs to a superconducting phase which does not connect to the high-temperature superconducting phase located near the AFM region of the temperature-substitution phase diagram. Instead this superconducting phase is "conventional" in the sense that superconductivity emerges from a Fermi liquid-like normal state. Since our study shows that the bandwidth renormalization of $LaRu_2P_2$ is negligible, a natural explanation for the mass enhancement observed in quantum oscillation experiments [6] is that the renormalization occurs only near E_F and is caused by an electron-bosonic mode interaction with the mode energy $\lesssim$ 80 meV, which is smaller than the energy resolution used in our SX-ARPES measurements. This is different to Fe-pnictides whose mass enhancement (by a factor of 2-3) results from bandwidth renormalizations and is attributed to electron-electron interaction [8, 14, 15].

We now emphasize that the increased probing depth in SX-ARPES, compared to widely used UV-ARPES, is critical in revealing the bulk electronic structure of $LaRu_2P_2$. For comparison we plot in Fig. 4(a) a UV-ARPES spectrum along the Γ-M direction acquired using circularly polarized light with $h\nu = 74$ eV (data measured with s- and p-polarized light show similar behavior). The bands indicated by arrows, which do not appear in SX-ARPES spectra (Fig. 3 (a)-(b)), cannot be identified with the bulk electronic structure from the DFT calculation. The dispersion of these bands does not change with photon energies in the range of 28 - 88 eV which corresponds to a k_z range covering more than one BZ (Fig. 4(c)-(e)). This suggests that these new bands origi-

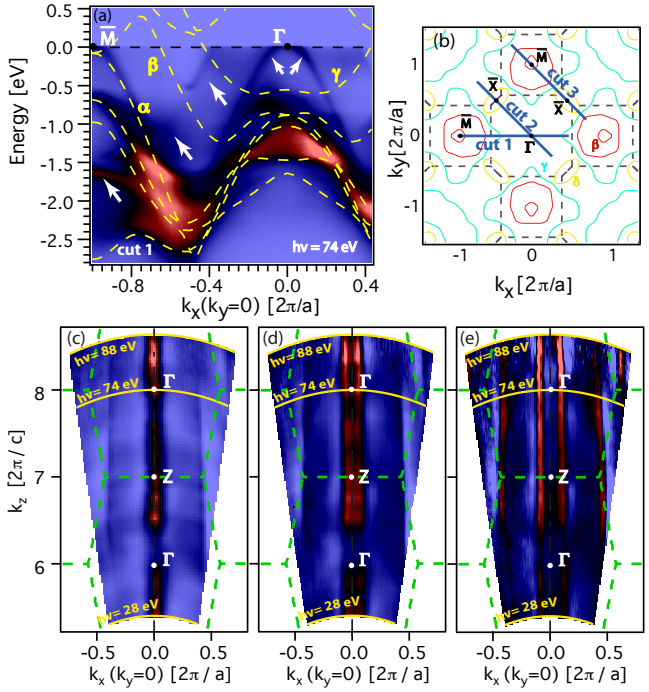

FIG. 4: (Color online) Band dispersion in $LaRu_2P_2$ measured with UV-ARPES. (a) UV-ARPES spectrum along the M-Γ direction (cut 1 in (b)) taken with $h\nu = 74$ eV. The superimposed dashed lines are the band structure from the DFT calculation. (b) DFT Fermi surface for $h\nu = 615$ eV. (c)-(e) Intensity map in (k_x,0,k_z) plane, taken with $h\nu = 28 - 88$ eV in steps of 2 eV. The maps are obtained by integrating ARPES spectral weight in an energy window of $E_F \pm 10$ meV, ($E_F - 100$ meV) $\pm$ 10meV and ($E_F - 200$ meV) $\pm$ 10 meV, respectively.

nate from the surface layer and do not represent the bulk electronic structure. Since LEED shows a clear (1×1) pattern [8], we conclude that the additional bands observed with UV-ARPES may have the same origin as those in the "1111" Fe-pnictides [22], where they result from the surface and subsurface layers due to surface relaxation. It is interesting to note that some FS pockets of $BaFe_2As_2$ observed by UV-ARPES are absent in the FS obtained from bulk-sensitive Shubnikov-de Haas oscillation measurements [14]. Moreover it has been reported that the energy bands obtained from UV-ARPES on $BaFe_{2-x}Co_xAs_2$ are significantly distorted with respect to the bulk electronic structure [23]. It will be important to re-visit Fe-pnictides with SX-ARPES to clarify this controversy. It will be vital for the community to gain confidence in ARPES results on the bulk electronic structure of these materials, especially for those studies for which there is no independent experimental check on bulk electronic structure, such as quantum oscillation experiments, for example on type-II superconductors with large H_{c2} values.

In summary, using SX-ARPES we revealed the electronic structure in the normal state of the "122" Pnictide superconductor ($LaRu_2P_2$), which is in significant agreement with DFT calculations. The negligible renormalization of the bandwidth suggests that the mass enhancement observed in quantum oscillation experiments is due to electron-boson coupling and is limited to narrow range ($\lesssim 80$ meV) around the E_F. Our results suggest that the origin of the superconducting phase in $LaRu_2P_2$ is different from the one in the "122" Fe-pnictides and more "conventional" in the sense that it emerges from a Fermi liquid-like normal state. By comparing with UV-ARPES spectra, we have illustrated that the increased probing depth of SX-ARPES is essential for the determination of bulk electronic structure in our experiments.

We are grateful to P. J. W. Moll and B. Batlogg for useful discussions. M.K. acknowledges support from the Japan Society for the Promotion of Science. This work was supported by the Swiss National Science Foundation through NCCR MaNEP. This work was performed at SLS of the Paul Scherrer Institut, Villigen PSI, Switzerland. We thank the beam line staff of ADRESS and of SIS for their excellent support.

[1] Y. Kamihara et al., J. Am. Chem. Soc. 130, 3296 (2008).
[2] W. Jeitschko *et al.*, J. Sol. St. Chem. 69, 93 (1987).
[3] S. Kasahara *et al.*, Phys. Rev. B 81, 184519 (2010).
[4] S. Sharma *et al.*, Phys. Rev. B 81, 174512 (2010).
[5] W. Jeitschko *et al.*, Z. Anorg. Allg. Chem. 527, 73 (1985).
[6] P. J. W. Moll *et al.*., Phys. Rev. B 84, 224507 (2011).
[7] J. Paglione and R. L. Greene, Nat. Phys. 6, 645 (2009).
[8] See Supplemental Material at [URL will be inserted by publisher] for further details on the experiments and on the discussion on the mass enhancement.
[9] P. Hohenberg and W. Kohn, Phys. Rev. 136, B864 (1964).
[10] B. Delley, J. Chem. Phys. 92, 508 (1990); B. Delley, J. Chem. Phys. 113, 7756 (2000).
[11] D. J. Singh, Phys. Rev. B 78, 094511 (2008).
[12] S. Hüfner, Photoelectron Spectroscopy (Springer, Berlin, 1995).
[13] J. G. Analytis *et al.*, Phys. Rev. Lett. 103, 076401 (2009).
[14] T. Terashima *et al.*, Phys. Rev. Lett. 107, 176402 (2011).
[15] P. Richard *et al.*, Rep. Prog. Phys. 74, 124512 (2011).
[16] P. Fazekas, Lectures notes on electron correlation and magnetism (World Scientific, Singapore, 1999).
[17] E. Şaşioğlu, C. Friedrich and S. Blügel, Phys. Rev. B 83, 121101(R) (2011).
[18] H. Ishida and A. Liebsch Phys. Rev. B 81, 054513 (2010).
[19] V. Brouet *et al.*, Phys. Rev. Lett. 105, 087001 (2010).
[20] H. Shishido *et al.*, Phys. Rev. Lett. 104, 057008 (2010).
[21] Y. Muraba *et al.*, Phys. Rev. B 82, 180512 (R) (2010).
[22] H. Eschrig, A. Lankau, and K. Koepernik, Phys. Rev. B 81, 155447 (2010).
[23] E. van Heumen *et al.*, Phys. Rev. Lett. 106, 027002 (2011).
[24] A. Kokalj, Comp. Mater. Sci., 2003, Vol. 28, p. 155. Code available from http://www.xcrysden.org/.